

Compressed *Gaussian* likelihood for the *Planck* low- ℓ data

Nanoom Lee^{1,*}

¹*William H. Miller III Department of Physics & Astronomy,
Johns Hopkins University, Baltimore, Maryland 21218, USA*

(Dated: June 4, 2026)

We present a compressed *Gaussian* likelihood for the *Planck* CMB low- ℓ E-mode polarization data, constructed from the `Sro112` likelihood which provides the tightest constraint on the reionization optical depth τ to date. The non-Gaussian form of CMB low- ℓ TT and EE likelihoods makes them incompatible with Fisher matrix analyses that require an analytic Gaussian χ^2 , such as the Fisher-bias formalism and Fisher forecasts. We show that the χ^2 of an offset log-normal likelihood takes a Gaussian form in the log-transformed power spectrum amplitudes, and can therefore serve as a proxy for the true Gaussian likelihood of this variable in Fisher matrix analyses, without any explicit change of variables. Building on this, we compress the `Sro112` likelihood into a small number of piecewise offset log-normal functions and validate it against the full `Sro112` likelihood via MCMC combined with *Planck* and ACT DR6 data, finding excellent agreement across all Λ CDM parameters and in extended cosmological models. We further demonstrate that Fisher matrix uncertainty estimates from our compressed likelihood agree well with the full MCMC posteriors. We release our compressed likelihood `planck-gaussian-lowl`, a lightweight Python package incorporating the compressed low- ℓ TT likelihood from previous work, allowing a straightforward incorporation of the *Planck* CMB low- ℓ data into any Gaussian-likelihood-based analysis. The package is publicly available at github.com/nanoomlee/planck-gaussian-lowl.

I. INTRODUCTION

The optical depth to reionization, τ , is one of the six standard parameters of the flat Λ CDM model. It is primarily constrained by Cosmic Microwave Background (CMB) E-mode polarization power spectrum on the large angular scales, which carries the imprint of Thomson scattering off free electrons during the epoch of reionization. An accurate and convenient likelihood for these data is therefore essential.

The *Planck* 2018 legacy release [1–3] included the `SimAll` likelihood for low- ℓ EE polarization, constructed from simulations of the *Planck* High Frequency Instrument (HFI) maps [4]. However, the 2018 maps are known to be affected by residual instrumental systematic effects, most notably from the nonlinear response of the analog-to-digital converters (ADCNL) of the HFI detectors [5]. The `Sro112` algorithm [5, 6] provides an improved map-making approach that better corrects these systematics, reducing the variance of the low- ℓ EE spectrum by a factor of two at $\ell < 6$ compared to the 2018 legacy maps. The resulting `Sro112` likelihood has therefore provided the tightest constraint on τ , which is $\tau = 0.0566_{-0.0062}^{+0.0053}$ at 68% confidence level.

The `Sro112` likelihood is distributed as a pre-tabulated probability table, providing the log-probability of the data as a function of D_ℓ^{EE} in units of $10^{-4}\mu\text{K}^2$ at each multipole from $\ell = 2$ to 29. As with all other CMB low- ℓ likelihoods, these probabilities are non-Gaussian, posing a challenge for analysis methods that assume an analytic Gaussian likelihood. Such methods include the Fisher-bias formalism [7–12] and the Fisher matrix forecasts for

future CMB surveys combined with existing *Planck* low- ℓ data. In practice, many analyses sidestep this issue by replacing the full `Sro112` likelihood with a simple Gaussian prior on τ or neglecting the low- ℓ data altogether. While convenient, this Gaussian prior discards the full shape information of the likelihood including its characteristic asymmetry and the correlation between τ and A_s . Neglecting the low- ℓ data, on the other hand, leaves τ essentially unconstrained, which can bias the inference of correlated parameters such as A_s and the neutrino mass [13, 14].

The non-Gaussian nature of CMB low- ℓ likelihoods and the associated difficulties for parameter estimation have been studied in Ref. [15]. The authors proposed the offset log-normal distribution as one of the approximations to the likelihood and showed that it is indeed an accurate approximation near the peak of the likelihood and working in the transformed variable yields an approximately Gaussian χ^2 , avoiding the systematic bias that arises from assuming Gaussianity in CMB spectra. This motivated Ref. [16] to perform log-normal fits for the posterior of low- ℓ TT and EE spectra compressing the *Planck commander* and `SimAll` likelihoods to facilitate the use of the likelihood in cosmological analyses.

In this paper, building on these earlier works and extending them in two ways, we present a compressed *Gaussian* likelihood for the `Sro112` low- ℓ EE data. First, and more importantly, we show that the χ^2 of an offset log-normal likelihood takes a Gaussian form in the log-transformed power spectrum amplitudes and can serve as a proxy for the true Gaussian likelihood of this variable in Fisher matrix analyses, without any explicit change of variables, as we show in Sec. III. This observation, which to our best knowledge has not been explicitly made before, directly justifies the approach used in ear-

* nanoom.lee@jhu.edu

lier work [12, 17–20] and makes the compressed likelihood directly compatible with Fisher matrix analyses that previously could not incorporate the non-Gaussian low- ℓ likelihood. Second, we introduce a piecewise offset log-normal fitting scheme that more accurately captures the asymmetric tails of the binned posteriors, which a single log-normal fails to reproduce. Note that while we focus on low- ℓ EE data in this work, the same Gaussian χ^2 structure applies to any offset log-normal compressed likelihood, including the low- ℓ TT likelihood of Ref. [16].

We validate the compressed likelihood against the full `Sroll2` likelihood by performing MCMC analysis combined with *Planck* and ACT DR6 data, replacing only the low- ℓ EE component. We find excellent agreement in the full Λ CDM posterior across all parameters, with no visible bias in the means and negligible differences in the 1σ uncertainties. We further demonstrate that Fisher matrix uncertainty estimates on τ and $\ln(10^{10}A_s)$ from our compressed likelihood agree well with the full MCMC posteriors, and validate the compressed likelihood in extended cosmological models including a non-flat Λ CDM model and a dark energy model with a time-varying equation of state (w_0, w_a), finding good agreement with the full `Sroll2` likelihood across all parameters in both cases. Our compressed *Gaussian* likelihood, `planck-gaussian-lowl`, is available at github.com/nanoomlee/planck-gaussian-lowl. Our package also incorporates the compressed low- ℓ TT likelihood of Ref. [16] in a consistent Gaussian χ^2 form.

The paper is organized as follows. In Sec. II we briefly describe the `Sroll2` likelihood. In Sec. III we derive the Gaussian χ^2 form of the offset log-normal likelihood and its connection to Fisher matrix analyses. In Sec. IV we describe our compression method in detail. In Sec. V we present the validation of our compressed likelihood. We conclude in Sec. VI.

II. THE SROLL2 LIKELIHOOD FOR PLANCK LOW- ℓ EE DATA

While the compression method we develop is general and applicable to any low- ℓ CMB likelihood, we apply it to the `Sroll2` likelihood, which we briefly describe here. The `Sroll2` likelihood [5] is based on the High Frequency Instrument (HFI) data of the *Planck* satellite, processed with the improved `Sroll2` mapmaking algorithm [6]. Compared to the *Planck* 2018 legacy maps, the `Sroll2` maps contain significantly lower levels of residual large-scale contamination, and provide roughly a factor of two tighter constraint on the reionization optical depth, $\tau = 0.0566^{+0.0053}_{-0.0062}$. In combination with *Planck* and ACT DR6 high- ℓ temperature and polarization data, it yields $\tau = 0.0603^{+0.0055}_{-0.0065}$ [21].

In the publicly available `Sroll2` likelihood, the posteriors of $D_\ell^{EE} \equiv \ell(\ell+1)C_\ell^{EE}/(2\pi)$ for $2 \leq \ell \leq 29$ are pre-tabulated on a discrete integer grid, $D_\ell^{EE} \in [0, 2999]$ with D_ℓ^{EE} in units of $10^{-4}\mu\text{K}^2$, and used to evaluate the

total likelihood given theoretical predictions for the CMB EE power spectrum. While each individual posterior is non-analytic, it roughly follows a log-normal form, motivating the compression approach we describe below.

III. GAUSSIAN χ^2 FROM A LOG-NORMAL LIKELIHOOD

In Bayesian statistics, the posterior distribution of parameters θ given data d is proportional to the likelihood function and the assumed prior,

$$p(\theta|d) \propto \mathcal{L}(d|\theta)p(\theta). \quad (1)$$

For the purpose of this section, $\theta \equiv D_\ell$ denotes the low- ℓ CMB angular power spectrum, and we consider the case where the posterior $p(\theta|d)$, obtained with a flat prior on θ , follows an offset log-normal distribution.¹ Specifically, the likelihood function takes the form

$$\mathcal{L}(d|\theta) = \frac{1}{(\theta - \theta_0)\sigma\sqrt{2\pi}} \exp\left[-\frac{(\ln(\theta - \theta_0) - \mu)^2}{2\sigma^2}\right], \quad (2)$$

where θ_0 is an offset, and μ and σ^2 are the mean and variance of the normal variable $\ln(\theta - \theta_0)$, i.e. $\ln(\theta - \theta_0) \sim \mathcal{N}(\mu, \sigma^2)$. Under the change of variable $x \equiv \ln(\theta - \theta_0)$, the likelihood for x is given by

$$\tilde{\mathcal{L}}(d|x) = \mathcal{L}(d|\theta) \left| \frac{d\theta}{dx} \right| = \frac{1}{\sigma\sqrt{2\pi}} e^{-(x-\mu)^2/2\sigma^2}, \quad (3)$$

which is exactly Gaussian, by definition. The corresponding χ^2 is

$$\tilde{\chi}^2(x) \equiv -2 \ln \tilde{\mathcal{L}}(d|x) = \frac{(x - \mu)^2}{\sigma^2}, \quad (4)$$

up to a constant. This is a standard quadratic form in $x = \ln(\theta - \theta_0)$, and is therefore directly compatible with any analysis framework that assumes a Gaussian χ^2 .

In practice, however, CMB likelihoods are provided as functions of the power spectra D_ℓ themselves, not of their logarithms. Furthermore, the offset in general is not known. The natural question is therefore whether one can work directly with $\mathcal{L}(d|\theta)$ rather than $\tilde{\mathcal{L}}(d|x)$. Rewriting the log-normal likelihood explicitly,

$$\begin{aligned} \mathcal{L}(d|\theta) &= \frac{1}{\sigma\sqrt{2\pi}} e^{-\ln(\theta - \theta_0)} e^{-[\ln(\theta - \theta_0) - \mu]^2/2\sigma^2} \\ &= \frac{1}{\sigma\sqrt{2\pi}} e^{-[\ln(\theta - \theta_0) - \tilde{\mu}]^2/2\sigma^2 + \sigma^2/2}, \end{aligned} \quad (5)$$

where $\tilde{\mu} \equiv \mu - \sigma^2$. The corresponding χ^2 is

$$\chi^2(\theta) \equiv -2 \ln \mathcal{L}(d|\theta) = \frac{[\ln(\theta - \theta_0) - \tilde{\mu}]^2}{\sigma^2}, \quad (6)$$

¹ The following arguments hold for the standard log-normal distribution (e.g., when $\theta_0 = 0$).

up to a constant. While $\chi^2(\theta)$ and $\tilde{\chi}^2(x)$ are not the same function — they differ by the shift $\mu \rightarrow \tilde{\mu} = \mu - \sigma^2$ and hence have different peaks due to the Jacobian [see Eq. (3)] — their second derivatives with respect to $x = \ln(\theta - \theta_0)$ are identical as the constant shift $\mu \rightarrow \tilde{\mu}$ drops out exactly under differentiation. Since the Fisher information matrix depends only on second derivatives of the χ^2 , it follows that one can use either $\tilde{\chi}^2(x)$ or $\chi^2(\theta)$ to compute the Fisher matrix, as long as derivatives are taken with respect to $x = \ln(\theta - \theta_0)$. Explicitly, the Fisher information for $x = \ln(\theta - \theta_0)$ is

$$\begin{aligned} F_{xx} &\equiv - \left\langle \frac{\partial^2 \ln \tilde{\mathcal{L}}(d|x)}{\partial x^2} \right\rangle = \frac{1}{2} \frac{\partial^2 \tilde{\chi}^2(x)}{\partial x^2} \\ &= \frac{1}{2} \frac{\partial^2 \chi^2(\theta)}{\partial [\ln(\theta - \theta_0)]^2}. \end{aligned} \quad (7)$$

The Fisher matrix for cosmological parameters p_i can then be obtained by

$$F_{ij} = \sum_{\ell, \ell'} \frac{\partial x_\ell}{\partial p_i} F_{x_\ell x_{\ell'}} \frac{\partial x_{\ell'}}{\partial p_j}, \quad (8)$$

where $x_\ell \equiv \ln(\theta_\ell - \theta_{0,\ell})$ and the sum runs over all ℓ modes (or bins) included in the likelihood.

This result has an important practical implication. While the **Sroll2** likelihood is provided as a non-analytic function of D_ℓ^{EE} , the compressed *Gaussian* likelihood we construct in Sec. IV provides $\chi^2(D_\ell^{EE})$ in the quadratic form of Eq. (6). This χ^2 serves as a proxy for the true Gaussian likelihood of $\ln(D_\ell - D_0)$ and can therefore be used directly in Fisher matrix analyses without any explicit change of variables.

We note that this way of incorporating the compressed low- ℓ EE (and TT) likelihood in the context of the Fisher-bias formalism was introduced in Ref. [12] and has been used in Refs. [17–20], but without explicitly showing that two different χ^2 functions, $\chi^2(\theta)$ and $\tilde{\chi}^2(x)$, have identical second derivatives with respect to $x = \ln(D_\ell - D_0)$, which justifies treating $\ln(D_\ell - D_0)$ as the effective parameter. The result above provides this justification.

In the following section, we show that the **Sroll2** low- ℓ EE likelihood can be well approximated in this quadratic form through piecewise offset log-normal fits to the binned posteriors, accurately capturing the full shape of the likelihood.

IV. CONSTRUCTING THE COMPRESSED GAUSSIAN LIKELIHOOD

We describe here the construction of our compressed *Gaussian* likelihood for the *Planck* low- ℓ EE data. The key observation is that offset log-normal fits to the binned D_ℓ^{EE} posteriors yield a χ^2 that takes a Gaussian form in the log-transformed power spectrum amplitudes, and can therefore serve as a proxy for the true Gaussian likelihood

of this variable in Fisher matrix analyses. We therefore refer to the resulting compressed representation as the *compressed Gaussian likelihood*.

A. Binning scheme

The **Sroll2** likelihood provides the conditional posterior $p(D_\ell^{EE} | D_\ell^{EE, \text{obs}})$ for each multipole $\ell = 2, \dots, 29$ separately, with D_ℓ^{EE} given in units of $10^{-4} \mu\text{K}^2$. Hereafter, we simply denote it as $p(D_\ell^{EE})$. Rather than working with all 28 individual posteriors directly, we group the multipoles into six bins \mathcal{B} ,

$$\mathcal{B} = \{\{2, 3\}, \{4, 5\}, \{6, 7\}, \{8-11\}, \{12-15\}, \{16-29\}\}, \quad (9)$$

and represent the joint likelihood with a fitted piecewise log-normal function per bin.

For a given bin i containing multipoles $\ell \in \mathcal{B}_i$, the binned log-likelihood is

$$\ln \mathcal{L}_i(\bar{D}_i^{EE}) = \sum_{\ell \in \mathcal{B}_i} \ln p(D_\ell^{EE} = \bar{D}_i^{EE}), \quad (10)$$

where \bar{D}_i^{EE} is the mean theoretical EE spectrum $D_\ell^{EE, \text{th}}$ over the bin,

$$\bar{D}_i^{EE} \equiv \frac{1}{|\mathcal{B}_i|} \sum_{\ell \in \mathcal{B}_i} D_\ell^{EE, \text{th}}. \quad (11)$$

The choice of binning scheme directly affects the fidelity of the compressed likelihood. For example, while wider bins produce smoother posteriors that are easier to fit, they mix multipoles that may prefer different D_ℓ^{EE} values, causing peak shifts and degrading compression accuracy. After exploring many possible binning schemes, we find that the 6-bin scheme defined in Eq. (9) works well in practice. The bins are illustrated in Fig. 1. We verified that finer binning does not significantly improve the fidelity of the compressed likelihood, mainly because narrower bins produce noisier posteriors that are harder to fit accurately with a log-normal function, resulting in a larger number of parameters without a commensurate gain in accuracy.

We demonstrate in Sec. V that the 6-bin scheme adopted here accurately reproduces the posterior distributions of all Λ CDM parameters when combined with *Planck* and ACT DR6 data.

B. Piecewise offset log-normal fit

For each bin i , we fit the binned log-likelihood $\ln \mathcal{L}_i(\bar{D}_i^{EE})$ with an offset log-normal function. The offset log-normal likelihood for bin i is

$$\mathcal{L}_i^{\text{fit}}(\bar{D}_i^{EE}) = \frac{1}{(\bar{D}_i^{EE} - D_{0,i}) \sigma_i \sqrt{2\pi}} e^{-\frac{[\ln(\bar{D}_i^{EE} - D_{0,i}) - \mu_i]^2}{2\sigma_i^2}}, \quad (12)$$

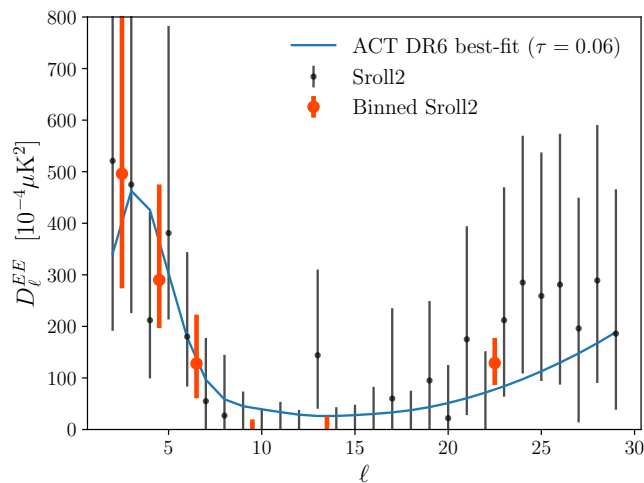


FIG. 1. The *Planck* low- ℓ EE power spectrum from the `Sroll2` likelihood (black points), compared to the ACT DR6 best-fit Λ CDM spectrum with $\tau = 0.06$ (blue curve). The black points mark the maximum likelihood values of the individual D_ℓ^{EE} posteriors, with error bars indicating the 1σ credible intervals. The red points show the corresponding quantities for the binned posteriors used in our compressed likelihood. The reionization bump is clearly visible at $\ell \lesssim 6$.

where $D_{0,i}$ is an offset ensuring $\bar{D}_i^{EE} > D_{0,i}$, and μ_i and σ_i are parameters characterising the shape of the distribution. Up to a constant, the log of this fitting function takes the form

$$\ln \mathcal{L}_i^{\text{fit}}(\bar{D}_i^{EE}) = -\frac{[\ln(\bar{D}_i^{EE} - D_{0,i}) - \tilde{\mu}_i]^2}{2\sigma_i^2}, \quad (13)$$

where $\tilde{\mu}_i \equiv \mu_i - \sigma_i^2$. The offset log-normal provides a natural fitting function for the binned D_ℓ^{EE} posteriors because the CMB power spectrum estimators \hat{C}_ℓ follow a scaled chi-squared distribution with $2\ell + 1$ degrees of freedom, and the log-normal distribution is known to provide an accurate approximation to the chi-squared distribution [15].²

We determine the fit parameters by minimising the likelihood-weighted sum of squared log-likelihood residuals,

$$\int d\bar{D}_i^{EE} \mathcal{L}_i(\bar{D}_i^{EE}) [\ln \mathcal{L}_i(\bar{D}_i^{EE}) - \ln \mathcal{L}_i^{\text{fit}}(\bar{D}_i^{EE})]^2, \quad (14)$$

where the integral is taken over a specified fitting range. This loss function emphasises accuracy where \mathcal{L}_i is large. While a single offset log-normal provides a reasonable approximation near the peak, it fails to capture the correct

² Other functional forms such as the offset chi-squared distribution could also serve as fitting functions. However, we use the offset log-normal as it yields a Gaussian χ^2 in $\ln(\bar{D}_i^{EE} - D_{0,i})$ up to a constant, as shown in Sec. III and Eq. (13).

shape of the tails. This can be seen from the blue dash-dotted curve in the top panels of Fig. 2, which is fitted over the $\pm 1\sigma$ region of the binned posterior.

To address this, we introduce a *piecewise* offset log-normal fit. For each bin, we divide the range of \bar{D}^{EE} into multiple regions, each fitted with a separate offset log-normal of the form Eq. (13). One piece containing the peak — which we call the central piece — is fitted freely by minimising Eq. (14) over a specified range. All remaining pieces are constrained by requiring that both $\ln \mathcal{L}_i^{\text{fit}}$ and its first derivative with respect to \bar{D}^{EE} are continuous at each junction. These two continuity conditions constrain two of the three parameters of each adjacent piece analytically in terms of the parameters of the preceding piece and the junction location, leaving one free parameter to be determined by minimising Eq. (14) over the corresponding region. That is, for an N -piece scheme, there are $N + 2$ fitting parameters in total.

We adopt the following piecewise scheme.³ For bins 1, 2, and 3 ($\ell = 2-3, 4-5, 6-7$), which have broader and more asymmetric posteriors, we use a 4-piece scheme where the central piece is fitted over the $(-1\sigma, +1\sigma)$ region:

- Piece 1: $(D_{-3\sigma}, D_{-1\sigma})$ — left tail, constrained from central at $D_{-1\sigma}$
- Piece 2: $(D_{-1\sigma}, D_{+1\sigma})$ — central, freely fitted
- Piece 3: $(D_{+1\sigma}, D_{+2\sigma})$ — constrained from central at $D_{+1\sigma}$
- Piece 4: $(D_{+2\sigma}, D_{+5\sigma})$ — constrained from piece 3 at $D_{+2\sigma}$

For bins 4, 5, and 6, which have smoother and more symmetric posteriors, we use a 2-piece scheme where the central piece is fitted over the $(-3\sigma, +3\sigma)$ region:

- Inner: $(D_{-3\sigma}, D_{+3\sigma})$ — central, freely fitted
- Outer: $(D_{+3\sigma}, D_{+5\sigma})$ — constrained from inner at $D_{+3\sigma}$

For the outermost pieces, the fitting range extends to the 5σ threshold of the binned posterior. For bins 1–3, the posterior does not reach this threshold within the tabulated `Sroll2` grid, so the fitting range extends to the edge of the probability table. The fitted parameters for all bins are summarised in Table I, and the fitted piecewise offset log-normal fits are shown in Fig. 2. As can be seen in Fig. 2, the piecewise fits accurately capture both the peak and the tails of the true binned posteriors.

³ Note that the fitting ranges specified here are used only to determine the free parameter of each piece. Once all parameters are determined, the piecewise function is evaluated using the junction locations as boundaries, with the leftmost piece covering all \bar{D} below the left junction and the rightmost piece covering all \bar{D} above the right junction. In cases where a junction crossing falls outside the tabulated `Sroll2` grid, the fitting range is truncated at the grid boundary.

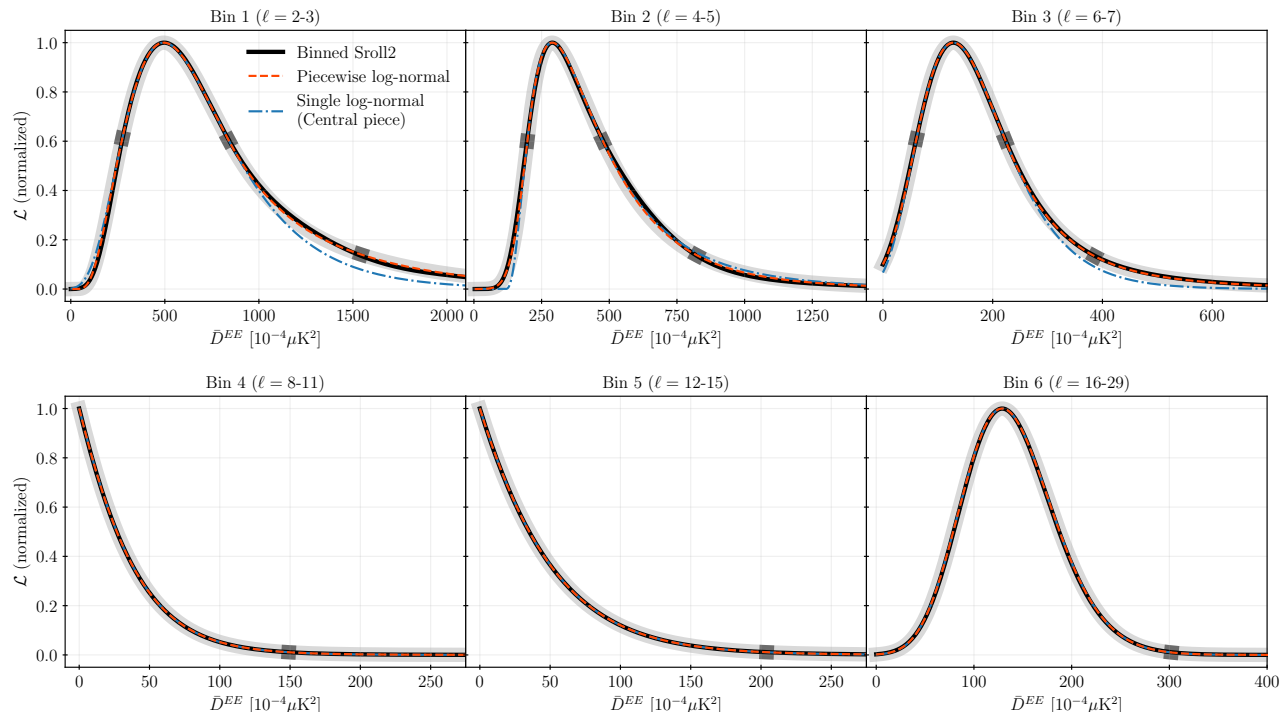


FIG. 2. Normalized likelihood $\mathcal{L}_i(\bar{D}_i^{EE})$ for each of the six bins (black solid), compared to the piecewise offset log-normal fit (orange dashed) and the single offset log-normal fitted over the $\pm 1\sigma$ region for bins 1–3 and the $\pm 3\sigma$ region for bins 4–6 (blue dash-dotted). The single log-normal fit shown corresponds to the central piece of the piecewise fit. The junction locations between adjacent pieces are indicated by dark grey squares. The piecewise fit accurately captures both the peak and the tails of the true binned posterior, while the single log-normal significantly under(over)estimates the high- \bar{D}^{EE} tail for bins 1 and 3 (bin 2).

C. Implementation as a Gaussian χ^2

As shown in Sec. III, the offset log-normal likelihood serves as a proxy for the true Gaussian likelihood of $\ln(\bar{D}_i^{EE} - D_{0,i})$. For the piecewise scheme, within each piece the log-likelihood takes the quadratic form of Eq. (13), so the total χ^2 is

$$\chi^2 = \sum_{i=1}^6 \left[\frac{[\ln(\bar{D}_i^{EE} - D_{0,i}^{(k)}) - \tilde{\mu}_i^{(k)}]^2}{(\sigma_i^{(k)})^2} + \Delta_i^{(k)} \right], \quad (15)$$

where the superscript (k) denotes the piece selected for bin i based on the value of \bar{D}_i^{EE} relative to the junction points, and $\Delta_i^{(k)}$ is a constant offset determined by requiring continuity of the χ^2 at each junction.

For Fisher matrix analyses, which are performed around the peak of the likelihood, it suffices to use only the central piece parameters. Since the central piece is specifically designed to accurately describe the curvature of the log-likelihood near the peak (see Appendix A), up to a constant the χ^2 reduces to

$$\chi_{\text{Fisher}}^2 = \sum_{i=1}^6 \frac{[\ln(\bar{D}_i^{EE} - D_{0,i}^{\text{central}}) - \tilde{\mu}_i^{\text{central}}]^2}{(\sigma_i^{\text{central}})^2}, \quad (16)$$

where the superscript “central” denotes the parameters of the central piece. This form is directly usable in

any analysis framework that assumes a Gaussian χ^2 , including the Fisher-bias formalism [7–12], by treating $\ln(\bar{D}_i^{EE} - D_{0,i}^{\text{central}})$ as the effective parameter for each bin.

V. VALIDATION

We validate our compressed *Gaussian* likelihood against the *Sroll2* likelihood by performing MCMC analysis using Cobaya [22] and CLASS [23], assuming the standard flat Λ CDM model. We use the parameter settings for CLASS suggested by the ACT Collaboration⁴ using HYREC-2 [24–26] as the recombination module. In both MCMC runs, we include the *Planck* low- ℓ TT likelihood, the *Planck* high- ℓ temperature and polarization likelihood, and the ACT DR6 likelihood (ACT-lite), replacing only the low- ℓ EE component with either the *Sroll2* likelihood or our compressed Gaussian likelihood.⁵ We sample all six standard Λ CDM parameters

⁴ github.com/ACTCollaboration/DR6_Notebooks/blob/main/ACT_DR6_ps_likelihood.ipynb

⁵ This likelihood combination is equivalent to P-ACT in Ref. [21], except that we use ACT-lite instead of the full multi-frequency ACT DR6 likelihood.

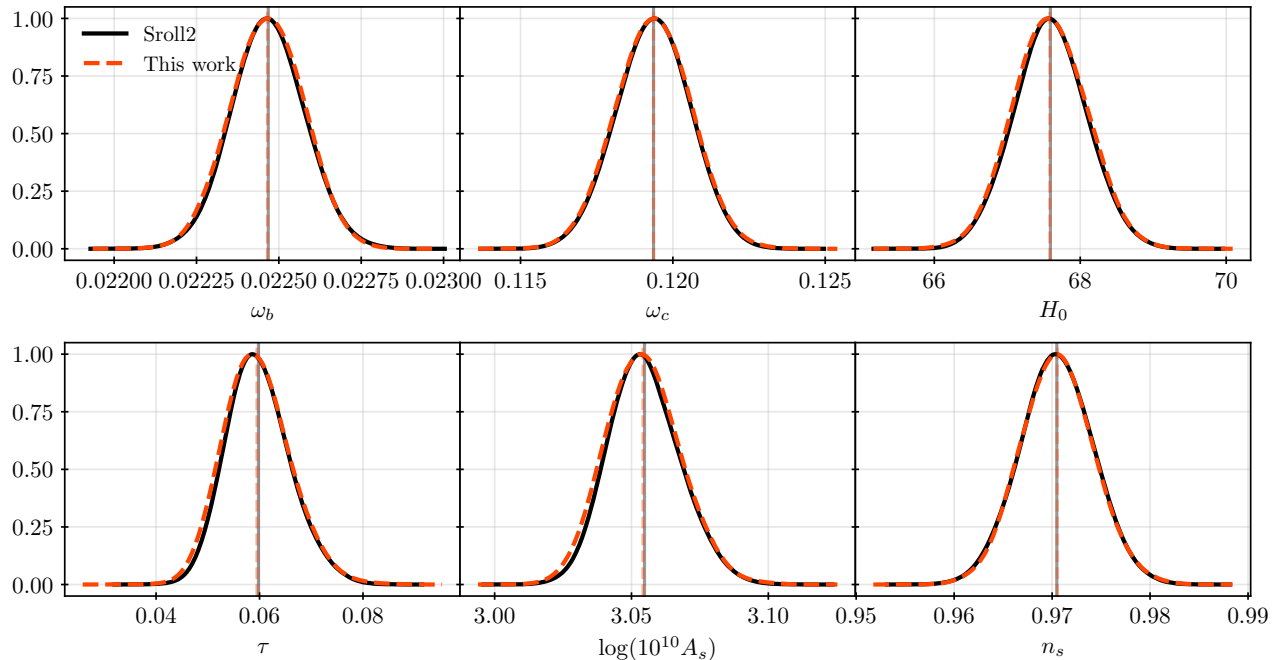


FIG. 3. Marginalized posterior distributions of the six Λ CDM parameters from MCMC analyses using the full *Sroll2* likelihood (black solid) and our compressed *Gaussian* likelihood (orange dashed), combined with *Planck* low- ℓ TT, *Planck* high- ℓ , and ACT DR6 data. Vertical lines indicate the respective posterior means. The two likelihoods are in excellent agreement across all parameters, validating the fidelity of our compression.

Bin	Piece	Fitting range	D_0	$\tilde{\mu}$	σ
Bin 1 ($\ell = 2-3$)	1	(72, 274)	7.304	6.246	0.666
	2	(274, 839)	-132.847	6.441	0.436
	3	(839, 1542)	414.517	5.047	0.999
	4	(1542, 2999)	-764.308	6.775	0.488
Bin 2 ($\ell = 4-5$)	1	(86, 197)	-526.882	6.672	0.087
	2	(197, 476)	107.656	5.201	0.701
	3	(476, 824)	47.510	5.452	0.603
	4	(824, 2999)	151.311	5.123	0.696
Bin 3 ($\ell = 6-7$)	1	(0, 61)	-406.681	6.269	0.122
	2	(61, 223)	-108.511	5.467	0.335
	3	(223, 386)	66.333	4.341	0.710
	4	(386, 2999)	133.968	3.721	0.900
Bin 4 ($\ell = 8-11$)	inner	(0, 149)	-136.446	4.526	0.352
	outer	(149, 514)	-28.144	3.358	0.567
Bin 5 ($\ell = 12-15$)	inner	(0, 204)	-228.794	4.967	0.333
	outer	(204, 743)	-43.811	3.586	0.581
Bin 6 ($\ell = 16-29$)	inner	(15, 302)	-208.849	5.822	0.136
	outer	(302, 479)	41.547	4.751	0.267

TABLE I. Fitted parameters of the piecewise offset log-normal likelihood for the 6-bin scheme adopted in this work. D_0 , $\tilde{\mu}$, and σ are the parameters of each piece, as defined in Eq. (12). Note that we work with D_ℓ^{EE} in units of $10^{-4} \mu\text{K}^2$, and both the fitting ranges and fitted parameters depend on this choice of unit.

$\{\omega_b, \omega_c, H_0, \tau, \ln(10^{10} A_s), n_s\}$, along with the ACT and *Planck* calibration parameters A_{ACT} and A_{Planck} .⁶

The resulting marginalized posterior distributions are shown in Fig. 3. The posteriors from our compressed likelihood (orange dashed) are in excellent agreement with those from the original *Sroll2* likelihood (black solid) across all parameters. In particular, τ and $\ln(10^{10} A_s)$, which are most sensitive to the low- ℓ EE likelihood, show no statistically significant bias in the means and negligible differences in the widths. The remaining parameters ω_b , ω_c , H_0 , and n_s , which are primarily constrained by the high- ℓ data but are also correlated with τ and A_s , are equally well reproduced.

In addition, we demonstrate that our compressed likelihood provides accurate parameter uncertainty estimates through Fisher matrix analyses. Table II presents the 1σ uncertainties on τ and $\ln(10^{10} A_s)$ from both Fisher matrix and MCMC, under the same likelihood combination described above. This demonstrates that our compressed Gaussian χ^2 , evaluated at the fiducial cosmology, provides Fisher matrix uncertainty estimates in good agreement with the full MCMC posteriors, validating the Gaussian χ^2 formulation of Sec. III. In contrast, comput-

⁶ The *Sroll2* likelihood rescales the theoretical spectrum at each ℓ by dividing by A_{planck}^2 , where A_{planck} is an overall calibration nuisance parameter. Our compressed likelihood retains this convention for consistency when used in MCMC analyses, with $A_{\text{planck}} = 1$ as a default value.

ing the Fisher matrix from the `Sroll2` likelihood assuming Gaussianity in D_ℓ^{EE} overestimates the uncertainties, since this assumption does not correctly capture the curvature of the non-Gaussian likelihood in parameter space as expected.

	MCMC	σ_{Fisher} (this work)	σ_{Fisher} (Sroll2)
τ	$0.0601^{+0.00534}_{-0.00697}$	± 0.00587	± 0.0101
$\ln(10^{10} A_s)$	$3.055^{+0.0121}_{-0.0142}$	± 0.0114	± 0.0192

TABLE II. Comparison of 1σ uncertainties on τ and $\ln(10^{10} A_s)$ from MCMC and the Fisher matrix, using the same likelihood combination as in Fig. 3. The Fisher matrix uncertainties from our compressed Gaussian likelihood agree well with the MCMC results, while those computed from the `Sroll2` likelihood assuming Gaussianity in D_ℓ^{EE} overestimate the uncertainties. MCMC constraints are quoted as posterior means with asymmetric 68% credible intervals; Fisher matrix uncertainties are symmetric by construction.

We further validate the compressed likelihood beyond the standard flat Λ CDM model. For a non-flat Λ CDM model and a dark energy model with a time-varying equation of state (w_0, w_a), our compressed likelihood yields posteriors consistent with the `Sroll2` likelihood across all parameters, with mean shifts $\lesssim 0.1\sigma$. We note that these small shifts may partly reflect the fact that extended models can shift the τ posterior relative to the flat Λ CDM case, causing the sampler to explore regions where the log-normal approximation is slightly less accurate than near the peak. Nevertheless, the $\lesssim 0.1\sigma$ level agreement demonstrates that the compressed likelihood remains a reliable tool beyond the standard Λ CDM model. We also emphasize that the primary purpose of this compressed likelihood is not to perfectly reproduce the `Sroll2` likelihood throughout the entire parameter space, but rather to provide an accurate Gaussian χ^2 near the peak for Fisher matrix analyses.

VI. CONCLUSION

We have presented a compressed *Gaussian* likelihood for the *Planck* low- ℓ EE polarization data, constructed from the `Sroll2` likelihood which currently provides the tightest constraint on the reionization optical depth τ . The key observation is that fitting the binned D_ℓ^{EE} posteriors with offset log-normal functions [Eq. (12)] yields a χ^2 that takes a Gaussian form in the log-transformed power spectrum amplitudes [Eq. (15)], and can therefore serve as a proxy for the true Gaussian likelihood of this variable in Fisher matrix analyses, without any explicit change of variables. This makes our compressed likelihood directly compatible with any analysis framework that requires an analytic Gaussian χ^2 , without any approximation beyond the log-normal fit itself. Exam-

ples include the Fisher-bias formalism [7–12] and Fisher matrix forecasts for future CMB surveys combined with existing *Planck* low- ℓ data.

To accurately capture the asymmetric tails of the binned posteriors, which a single offset log-normal fails to reproduce, we introduce a piecewise fitting scheme in which the range of the binned spectra is divided into multiple regions each fitted with a separate offset log-normal. The central piece containing the peak is fitted freely, and all adjacent pieces are constrained by requiring continuity of both the log-likelihood and its first derivative at each junction, leaving only one free parameter per piece. We fit each piece by minimising the likelihood-weighted sum of squared log-likelihood residuals [Eq. (14)], which prioritises accuracy near the peak of the distribution.

We validate the compressed likelihood against the `Sroll2` likelihood in three ways. First, we perform MCMC analysis combined with *Planck* and ACT DR6 data under the standard flat Λ CDM model, replacing only the low- ℓ EE component. The compressed likelihood reproduces the posterior distributions of all six Λ CDM parameters in excellent agreement with the `Sroll2` likelihood, with no visible bias in the means and negligible differences in the widths (Fig. 3). Second, we demonstrate that the Fisher matrix uncertainties on τ and $\ln(10^{10} A_s)$ computed from our compressed Gaussian χ^2 agree well with the MCMC posteriors, confirming that the Gaussian χ^2 formulation correctly captures the information content of the low- ℓ EE likelihood for Fisher matrix analyses (Table II). Third, we validate the compressed likelihood beyond the standard flat Λ CDM model, finding consistent posteriors with mean shifts $\lesssim 0.1\sigma$ for all parameters in both a non-flat Λ CDM model and a dark energy model with a time-varying equation of state (w_0, w_a).

Our compressed likelihood, `planck-gaussian-lowl`, is publicly available at github.com/nanoomlee/planck-gaussian-lowl as a lightweight Python package.⁷ The package incorporates the compressed low- ℓ TT likelihood of Ref. [16] in a consistent Gaussian χ^2 form, allowing users to straightforwardly combine both compressed low- ℓ TT and EE likelihoods. This package provides a simple and accurate tool for cosmological analyses that require a tractable analytic form of the low- ℓ EE likelihood, and we expect it to be broadly useful for CMB analyses.

ACKNOWLEDGMENTS

We thank Laura Herold and Benjamin Wandelt for useful discussions. NL was supported by the Horizon Fellowship from Johns Hopkins University. This work was carried out at the Advanced Research Computing at Hopkins (ARCH) core facility (rockfish.jhu.edu), which is supported by the National Science Foundation (NSF) grant number OAC1920103.

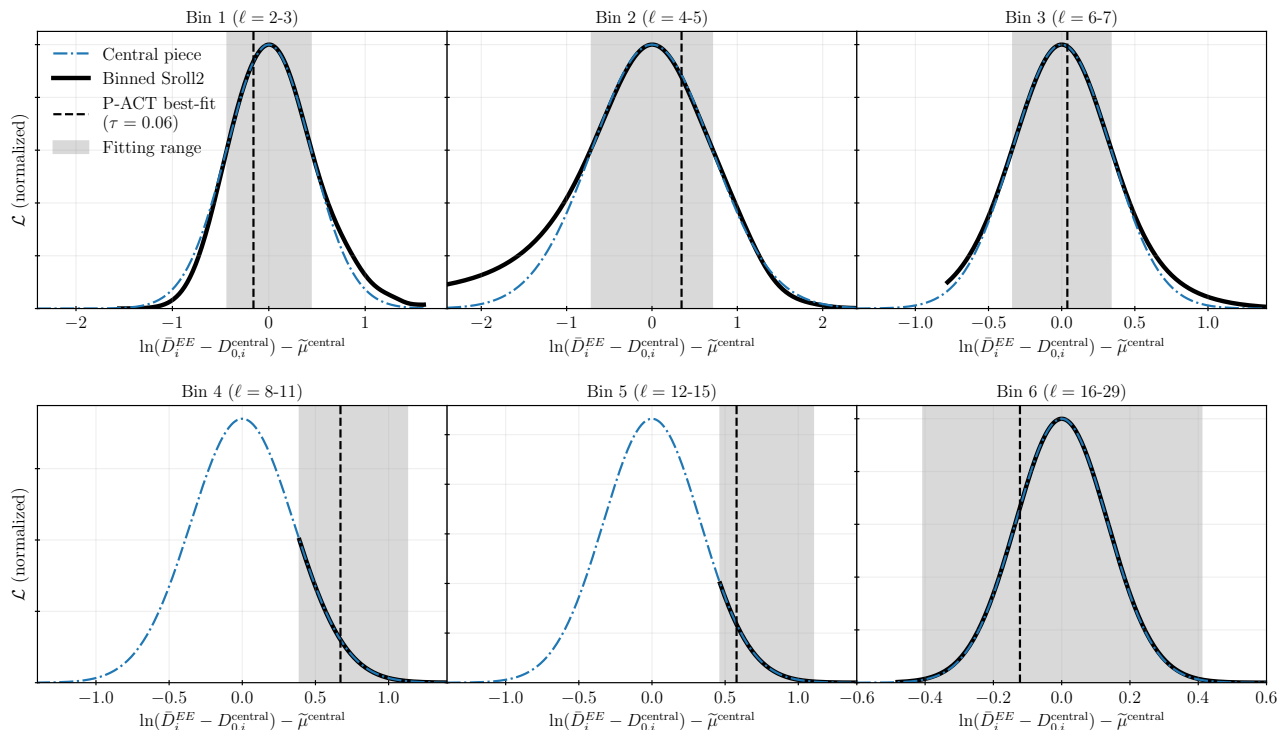


FIG. 4. Normalized likelihood $\mathcal{L}_i(\bar{D}_i^{EE})$ for each of the six bins (black solid) as a function of the transformed variable $\ln(\bar{D}_i^{EE} - D_{0,i}^{\text{central}}) - \tilde{\mu}_i^{\text{central}}$, where $D_{0,i}^{\text{central}}$ and $\tilde{\mu}_i^{\text{central}}$ are the parameters of the central piece. The central piece (blue dot-dashed) is exactly Gaussian in this variable by construction, peaked at zero, and is extended beyond the fitting range for illustration purposes. The shaded region indicates the fitting range of the central piece, within which the true `Sroll2` posterior closely follows the Gaussian shape, confirming that the central piece accurately captures the curvature of the likelihood near the peak and validating its use in Fisher matrix analyses [Eq. (16)]. The blue vertical line marks the P-ACT best-fit fiducial ($\tau = 0.06$), which falls within the fitting range for all bins.

Appendix A: Gaussian structure of the central piece

Figure 4 shows the normalized likelihood \mathcal{L}_i for each bin as a function of the transformed variable $\ln(\bar{D}_i^{EE} - D_{0,i}^{\text{central}}) - \tilde{\mu}_i^{\text{central}}$, where $D_{0,i}^{\text{central}}$ and $\tilde{\mu}_i^{\text{central}}$ are the parameters of the central piece. By construction, the central piece (blue, dot-dashed) is exactly Gaussian in this variable, peaked at zero, and is extended beyond the fitting range for illustration purposes. The

true `Sroll2` posterior (black) closely follows this Gaussian shape within the fitting range (shaded region), confirming that the central piece accurately captures the curvature of the likelihood near the peak, validating the use of this central piece to evaluate the Fisher matrix around the peak [Eq. (16)]. The blue vertical line shows the P-ACT best-fit fiducial ($\tau = 0.06$), which falls within the fitting range for all bins.

-
- [1] N. Aghanim *et al.* (Planck), *Astron. Astrophys.* **641**, A1 (2020), [arXiv:1807.06205 \[astro-ph.CO\]](#).
 - [2] N. Aghanim *et al.* (Planck), *Astron. Astrophys.* **641**, A6 (2020), [arXiv:1807.06209 \[astro-ph.CO\]](#).
 - [3] N. Aghanim *et al.* (Planck), *Astron. Astrophys.* **641**, A5 (2020), [arXiv:1907.12875 \[astro-ph.CO\]](#).
 - [4] N. Aghanim *et al.* (Planck), *Astron. Astrophys.* **641**, A3 (2020), [arXiv:1807.06207 \[astro-ph.CO\]](#).

- [5] L. Pagano, J. M. Delouis, S. Mottet, J. L. Puget, and L. Vibert, *Astron. Astrophys.* **635**, A99 (2020), [arXiv:1908.09856 \[astro-ph.CO\]](#).
- [6] N. Aghanim *et al.* (Planck), *Astron. Astrophys.* **596**, A107 (2016), [arXiv:1605.02985 \[astro-ph.CO\]](#).
- [7] L. Knox, R. Scoccimarro, and S. Dodelson, *Phys. Rev. Lett.* **81**, 2004 (1998), [arXiv:astro-ph/9805012](#).
- [8] A. G. Kim, E. V. Linder, R. Miquel, and N. Mostek, *Mon. Not. Roy. Astron. Soc.* **347**, 909 (2004), [arXiv:astro-ph/0304509](#).
- [9] A. N. Taylor, T. D. Kitching, D. J. Bacon, and A. F. Heavens, *Mon. Not. Roy. Astron. Soc.* **374**, 1377 (2007), [arXiv:astro-ph/0606416](#).

⁷ The repository includes the compressed likelihood module, an example Cobaya likelihood class for MCMC analyses, and an example script for Fisher matrix computation using the central piece parameters [Eq. (16)].

- [10] C. Shapiro, *Astrophys. J.* **696**, 775 (2009), [arXiv:0812.0769 \[astro-ph\]](#).
- [11] F. De Bernardis, R. Bean, S. Galli, A. Melchiorri, J. I. Silk, and L. Verde, *Phys. Rev. D* **79**, 043503 (2009), [arXiv:0812.3557 \[astro-ph\]](#).
- [12] N. Lee, Y. Ali-Haïmoud, N. Schöneberg, and V. Poulin, *Phys. Rev. Lett.* **130**, 161003 (2023), [arXiv:2212.04494 \[astro-ph.CO\]](#).
- [13] N. Sailer, G. S. Farren, S. Ferraro, and M. White, *Phys. Rev. Lett.* **136**, 081002 (2026), [arXiv:2504.16932 \[astro-ph.CO\]](#).
- [14] T. Jhaveri, T. Karwal, and W. Hu, *Phys. Rev. D* **112**, 043541 (2025), [arXiv:2504.21813 \[astro-ph.CO\]](#).
- [15] J. R. Bond, A. H. Jaffe, and L. E. Knox, *Astrophys. J.* **533**, 19 (2000), [arXiv:astro-ph/9808264](#).
- [16] H. Prince and J. Dunkley, *Phys. Rev. D* **105**, 023518 (2022), [arXiv:2104.05715 \[astro-ph.CO\]](#).
- [17] H. Plombat, T. Simon, J. Flitter, and V. Poulin, *JCAP* **01**, 071 (2025), [arXiv:2410.01486 \[astro-ph.CO\]](#).
- [18] S. H. Mirpoorian, K. Jedamzik, and L. Pogosian, (2024), [arXiv:2411.16678 \[astro-ph.CO\]](#).
- [19] N. Lee, M. Braglia, and Y. Ali-Haïmoud, *Phys. Rev. D* **112**, 083506 (2025), [arXiv:2504.07966 \[astro-ph.CO\]](#).
- [20] N. Lee and T. Zhou, In preparation.
- [21] T. Louis *et al.* (Atacama Cosmology Telescope), *JCAP* **11**, 062 (2025), [arXiv:2503.14452 \[astro-ph.CO\]](#).
- [22] J. Torrado and A. Lewis, *JCAP* **05**, 057 (2021), [arXiv:2005.05290 \[astro-ph.IM\]](#).
- [23] D. Blas, J. Lesgourgues, and T. Tram, *JCAP* **07**, 034 (2011), [arXiv:1104.2933 \[astro-ph.CO\]](#).
- [24] Y. Ali-Haimoud and C. M. Hirata, *Phys. Rev. D* **82**, 063521 (2010), [arXiv:1006.1355 \[astro-ph.CO\]](#).
- [25] Y. Ali-Haimoud and C. M. Hirata, *Phys. Rev. D* **83**, 043513 (2011), [arXiv:1011.3758 \[astro-ph.CO\]](#).
- [26] N. Lee and Y. Ali-Haïmoud, *Phys. Rev. D* **102**, 083517 (2020), [arXiv:2007.14114 \[astro-ph.CO\]](#).